Status Report on FINUDA Data Analysis, October 2007

The FINUDA OFFLINE Group

October 31, 2007

Abstract

A status report on the FINUDA analyses, performed on the data collected in the period November 2006-June 2007 and currently underway, is presented. The following topics will be touched: calibrations and alignments, hypernuclear spectroscopy, hypernuclei non-mesonic weak and rare decays, search for Neutron Rich Hypernuclei and Deeply Bound K^--nuclear states.

Contents

Chapter 1

Summary of 2006-2007 Data Taking

The 2006-2007 FINUDA data taking, after a period of machine tuning, started on Nov 20, 2006, and ended on June 6, 2007, with the collection of a total integrated luminosity of 966 pb^{-1}. During the data taking, in which the average daily luminosity delivered to FINUDA was 7 pb^{-1} (improving with time since the beginning of the run), the peak daily luminosity reached by the machine was 9.4 pb^{-1}.

Table 1.1 shows the amount of data collected by FINUDA during the full running time, according to the applied trigger, and reports, for comparison, the statistics collected in 2003-2004 with the same trigger conditions.

		2006-2007	2003-2004
Total collected luminosity		966 pb^{-1}	220 pb^{-1}
HYPE type triggers		210×10^6	29.7×10^6
BHABHA type triggers		32.8×10^6	7.5×10^6
cosmic ray data	B=0 T	8.8×10^6	5.5×10^6
	B=1 T	3.7×10^6	1.8×10^6

Table 1.1: Statistics collected in the 2006-07 data taking, compared to the 2003-2004 data taking (running since Dec. 1, 2003 to Mar. 23, 2004).

Chapter 2

Status of calibrations and alignments

2.1 Time calibrations

The Time Of Flight (TOF) system calibration was performed and completed, using K^+K^- events for the inner TOF array (TOFINO) and Bhabha events for the outer one (TOFONE). For TOFINO the time resolution achieved for the present data taking is $\sigma = 320$ ps, to be compared with $\sigma = 475$ ps obtained previously (we recall that the TOFINO hodoscope was replaced with one with thinner slabs and PM's instead of HPD's); for TOFONE it is $\sigma = 480$ ps, to be compared with the past $\sigma = 485$ ps (cables were changed and the electronics were re-tuned and refurbished, assuring much more stable operating conditions during the run). The stability of the time calibration was monitored over the full run.

For the other detectors, time calibrations for Low Mass Drift Chambers (LMDC in the following) were frequently updated already during the data taking; for straw tubes they were provided timely at the end of the run.

2.2 Charge calibrations

The fine charge calibration of the vertex module layers (ISIM and OSIM) is a delicate task and is being currently performed, also in the view of recovering information on highly ionizing particles. A first set of charge thresholds has been provided in order to allow particle identification (*p.id.*) by both the internal and external vertex detectors and tuned to avoid the loss of useful events.

2.3 Geometrical alignment

The alignment procedure was started, before the end of the run, already providing an initial correction of the macroscopic rotations and translations of the whole sets of inner and outer vertex detectors, and the two layers of low mass drift chambers. The following step, consisting to adjust module by module, was fulfilled by half July reaching a precision on the alignment of the vertex

detectors of about 80 μm. This situation was considered precise enough to start extracting the first physics results that will be presented in this report.

Finer tunings are of course still needed, module by module and taking modules in groups to understand possible interplays and shadowing effects in order to achieve the design resolution, and are programmed for the next last few months of 2007, and the first ones of 2008.

An accurate check of the design target position (that of course, in the alignment procedure, act as passive elements) was moreover performed improving the precision of the geometric description of the inner region.

The first alignment step allowed to correct the overall position of the vertex detector basket as seen from the straw tube system, considered as fixed in all our alignment procedures, giving a global rotation of ~ 0.024 rad, and a global translational offset along the longitudinal axis of -0.05 cm. The quality of the adjustments is verified inspecting the shape of the residual distributions obtained using straight cosmic rays (taken mainly at the beginning and end of data taking, and during the 2006 Christmas shutdown). The top line of Fig. 2.1 shows the raw distributions of residuals along the x and y local coordinates of the ISIM modules (evaluated with respect of the straw tube system), while the bottom ones are the same distributions after the application of the global rotation/translation: the improvement is clear.

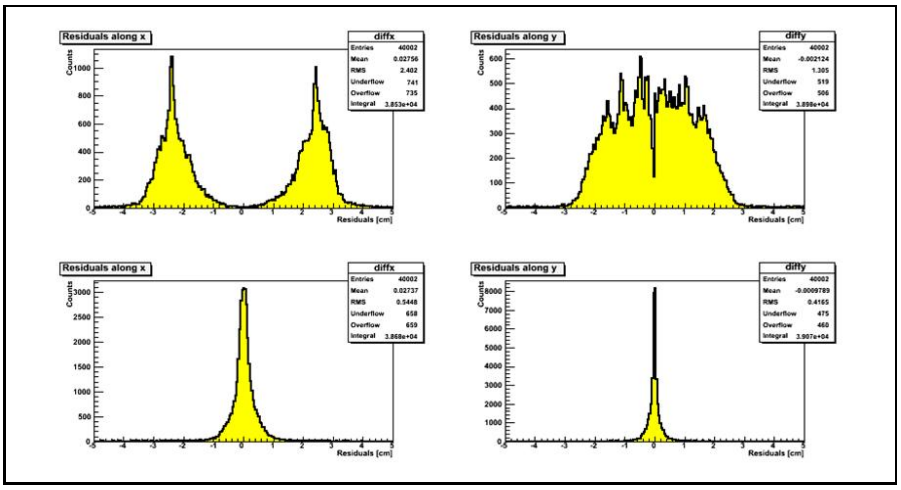

Figure 2.1: Residual along the local x coordinate (left) and along the local y one for all the ISIM modules before (top) and after (bottom) the global rotational and translational alignment.

Analogously, the top line of Fig. 2.2 shows the effect, from top to bottom, of the global alignment step for the LMDC's layers on the residual distributions along the ϕ and z coordinates: the plots show the necessity of a global translation of about 1 cm, that was also measured in the previous data taking.

The next step, consisting in a correction of the single module positions, is needed in order to heal situations like that shown in Fig. 2.3, top line: the residual distributions on a single vertex module may be heavily distorted due to the misplacement of the module itself as well as of all the other ones that are

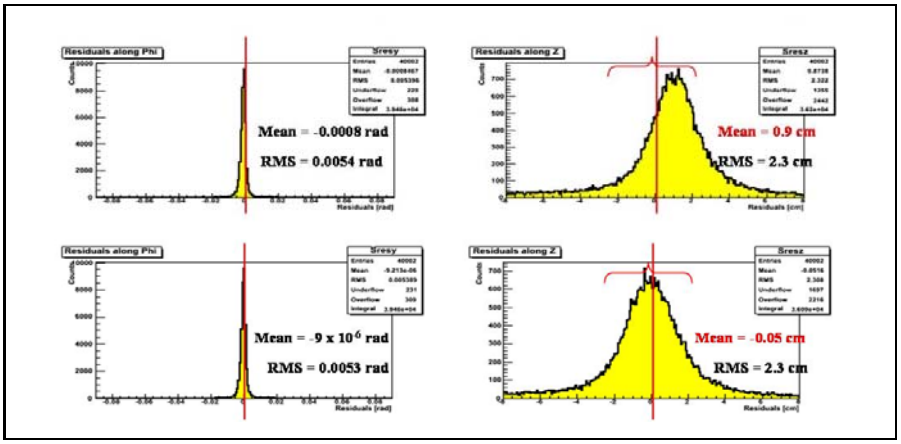

Figure 2.2: Residual along the ϕ coordinate (left) and along the z one for all the DCH1 modules before (top) and after (bottom) the global rotational and translational alignment. The red lines mark the expected mean value of the distributions.

used to infer the residual distribution on the module under study.

For this reason, this alignment phase is a very demanding and time-consuming job, which was temporarily suspended after a first survey and adjustment. The situation at the end of the first phase of the module-by-module alignment is shown in the bottom line of Fig. 2.3, in which the improvement achieved is already very sizeable.

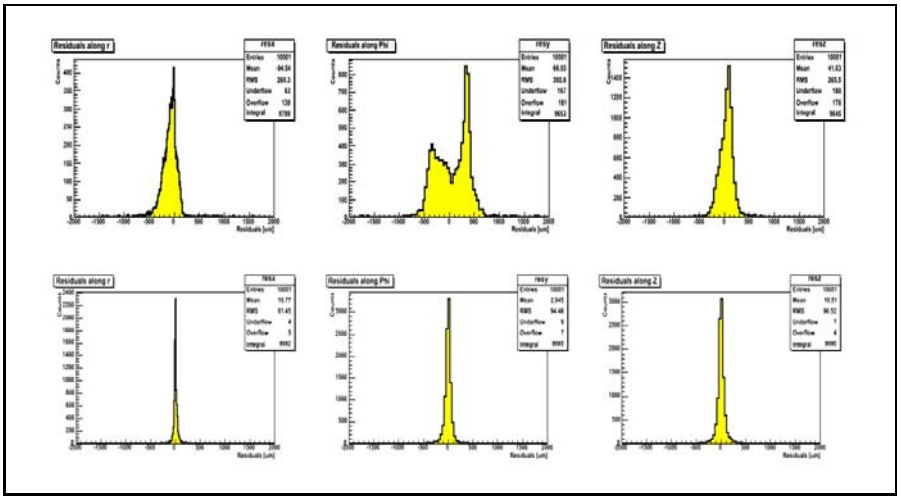

Figure 2.3: Residual along the r coordinate (left), the ϕ (center) and the z one (right) for one ISIM module before (top) and after (bottom) the single module alignment.

Chapter 3

Issues of current analyses

3.1 Present resolution: study of μ^+ momentum spectra

The study of the μ^+ momentum spectra, produced in the decay of K^+ in the targets, can give a useful tool to understand the behavior of the apparatus and possible distortion effects.

A first rough study can be made selecting long muon tracks (reconstructed with four points each) emerging from the eight targets. A more detailed study is based on the shape of muon spectra for particles emitted along selected paths, determined by different tracking detectors (OSIM-LMDC1-LMDC2 + straw triplet). In the second case, a more detailed study of the maximum achievable resolution may be performed, since each target subtends at least two different paths.

The muon spectra emitted by each target, integrated over the whole collected statistics, is shown in Fig. 3.1.

The tracks are selected to be long, well fitted and forward emitted. These spectra are useful mainly to understand the quality of the achieved correction for the geometrical misalignments.

The first four targets are located in the upper hemicylinder of the vertex cage: an up/down systematic asymmetry of the mean values cannot be stated. This asymmetry could have been connected to the problem of the air contamination of the Helium bag, that occurred during the data taking, affecting especially the lower sectors of the spectrometer, which face targets 6 and 7 respectively.

From this study no serious effect of the air contamination emerges, at the level or our present accuracy. A more detailed study of the air contamination should involve heavier particles (protons and deuterons), and is currently in progress.

Going into further detail, Fig. 3.2 shows the same momentum distributions for tracks selected in apparatus sectors, namely by "roads" corresponding to fractions of spectrometer octants. The figure reports the present situation for a chosen number of roads, that can be compared to what we obtained in a preliminary analysis during the data taking, presented to the Committee at end of February [1]. The improvement in the resolution due to vertex modules alignment and reconstruction code refinements is evident: the resolution, for

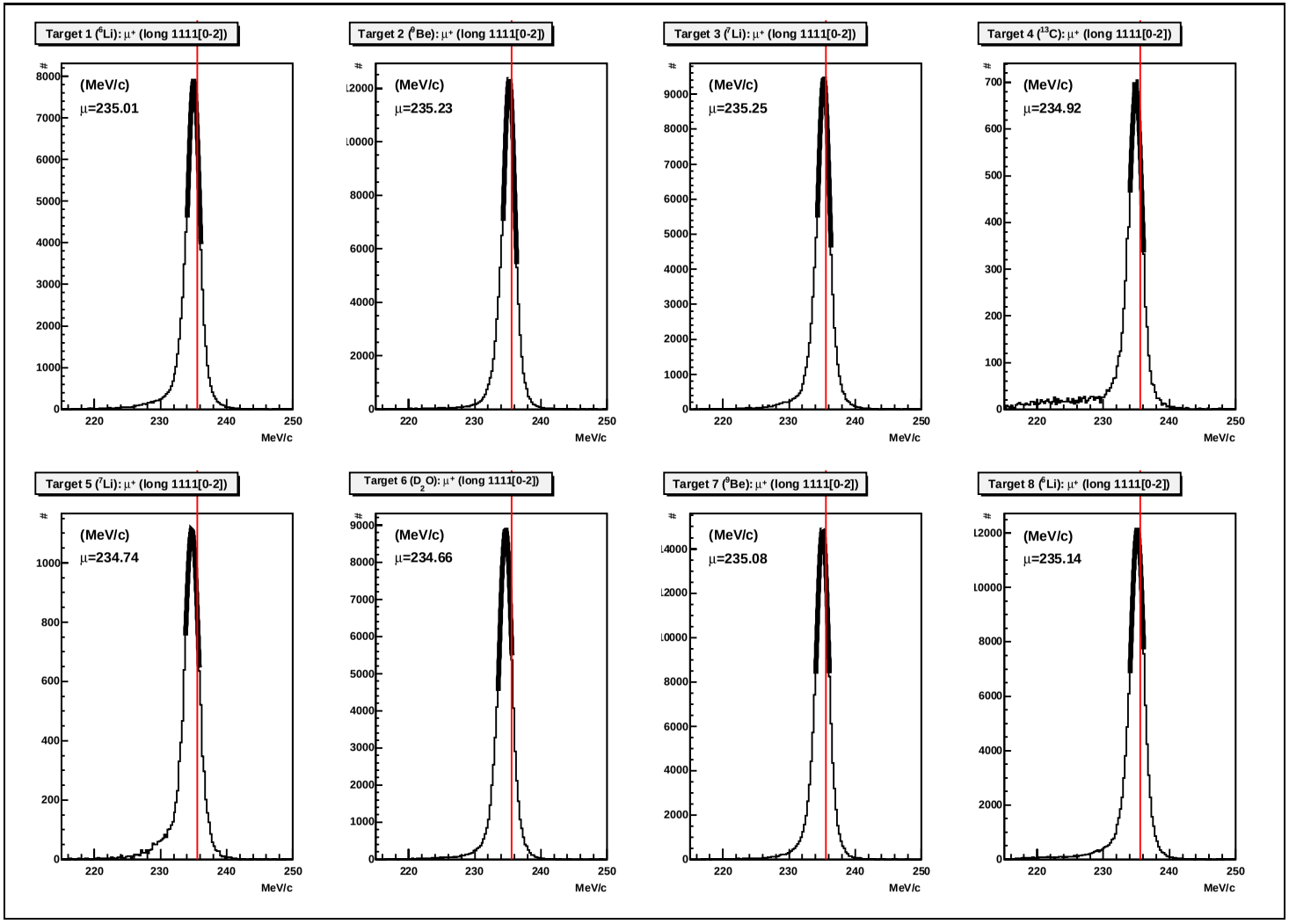

Figure 3.1: μ^+ momentum spectra from each target; all runs, forward long tracks selected. The red lines mark the μ^+ momentum nominal value for the $K_{\mu 2}$ decay.

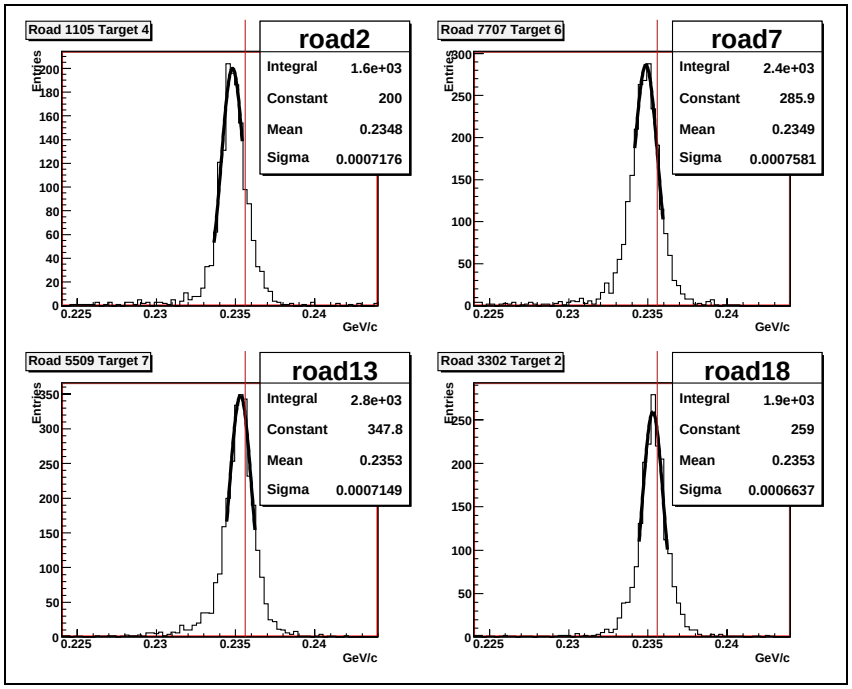

Figure 3.2: Distributions of the μ^+ momentum for tracks selected along different roads in the apparatus: top left, road 2, spanning the right part of the apparatus, with a resolution 0.72% FWHM); top right, road 7, spanning the bottom part of the apparatus (0.76% FWHM); bottom left, road 13, spanning the left part of the apparatus (0.71% FWHM); bottom right, road 18, spanning the upper part of the apparatus (0.66% FWHM). The evaluation was done on a sample of about 500 runs. The red lines mark the μ^+ momentum nominal value for the $K_{\mu 2}$ decay.

the same road, improves of a fraction of permil. The mean value, all over the data taking, is rather steady, and around 0.78%.

Further improvement is expected after completion of the alignment procedure.

3.2 Hypernuclear Spectroscopy

3.2.1 General overview

We recall that in the new data taking the target array was composed by two ^{6}Li and two ^{7}Li targets, already present in the 2003-2004 run, plus four new ones, namely two ^{9}Be, one ^{13}C and one D_2O. The latter were expected to deliver interesting results about the spectroscopy of new hypernuclear species, the former ones were used to increase the already available statistics for the study of non-mesonic weak decays of hyperfragments produced from the ^{6}Li target and for the spectroscopy of the $^7_\Lambda$Li hypernucleus.

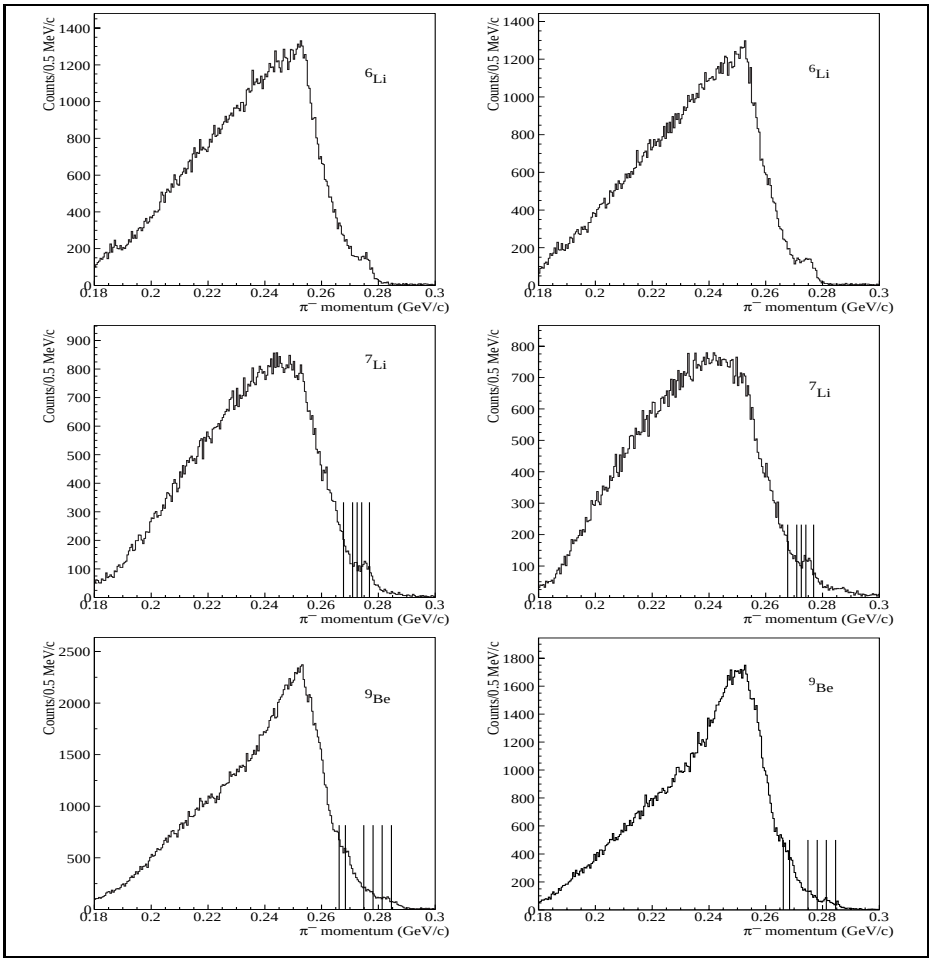

Figure 3.3: π^- inclusive momentum spectra for events with K^- stopping in ^{6}Li (top line), ^{7}Li (center line), and ^{9}Be (bottom line). Long, high resolution (four points) and forward tracks selected. The lines correspond to the momentum values for the formation of hypernuclear species (when possible).

An overview of the inclusive π^- momentum spectra from each of the eight targets is reported in Fig. 3.3 (for ^{6}Li, ^{7}Li and ^{9}Be targets) and Fig. 3.4

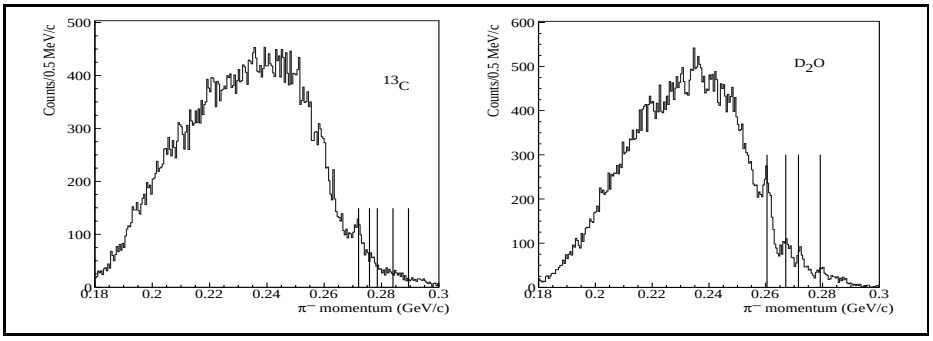

Figure 3.4: π^- inclusive momentum spectra for events with K^- stopping in ^{13}C (left) and ^{16}O (right). Long, high resolution (four points) and forward tracks selected. The lines correspond to the momentum values for the formation of hypernuclear species.

(^{13}C and ^{16}O targets). The tracks were selected to achieve the best available resolution: four points well fitted tracks, forward heading, with K^- vertex correctly reconstructed in the target volume. We can see that the quality and population of the spectra out of homologous targets is comparable, in spite of finer alignments still to be fulfilled.

The two spectra from ^{6}Li have a comparable shape to what we got in the first run, with a bump beyond 275 MeV/c, corresponding to the threshold for the formation of the ${}^{5}_{\Lambda}$He hyperfragment, in which the unstable ${}^{6}_{\Lambda}$Li decays by proton emission. These data are mainly useful for non-mesonic weak decay studies, as will be described in the following.

Concerning ${}^{7}_{\Lambda}$Li formation, we recall that in the first FINUDA data taking, in which just one target was available, the existence of two peaks, corresponding to two different hypernuclear levels separated in energy by 1.65 MeV, was observed. This was the first observation of a fine splitting of ${}^{7}_{\Lambda}$Li levels by means of a magnetic spectrometer [2]. Fig. 3.5 shows in closer detail the π^- spectrum obtained from one of the two targets available in the new run, with the application of much stronger selection cuts as compared to Fig. 3.3, with the purpose to observe a similar effect. Pending acceptance distortions and finer alignments, the double-peak structure may also be observed in the new data. We can count of an overall statistics at least 6 times larger than the previous one.

In spite of the huge statistics collected by two targets, the π^- spectra from ^{9}Be targets (last line in Fig. 3.3) show just feeble signals where the hypernuclear levels were expected, in the 268–285 MeV/c region, mainly in the form of small knees (except for a hint corresponding to the production of the ground state). The estimated capture rate [3] for these states was some $10^{-4}/\mathrm{K}^-_{stop}$: probably the real rate is even lower, and our sensitivity is not enough to disentangle them. It is interesting however to note the steepness of the rising left side, which is peculiar and similar for the ^{9}Be and ^{6}Li targets, while it rises much more softly for all the other ones. This feature deserves a detailed study: it might be related to the α-cluster substructures present in the two nuclei (namely, $(\alpha\alpha n)$ in ^{9}Be, (αd) in ^{6}Li).

Clear signals for the formation of ${}^{13}_{\Lambda}$C hypernuclear levels emerge correspond-

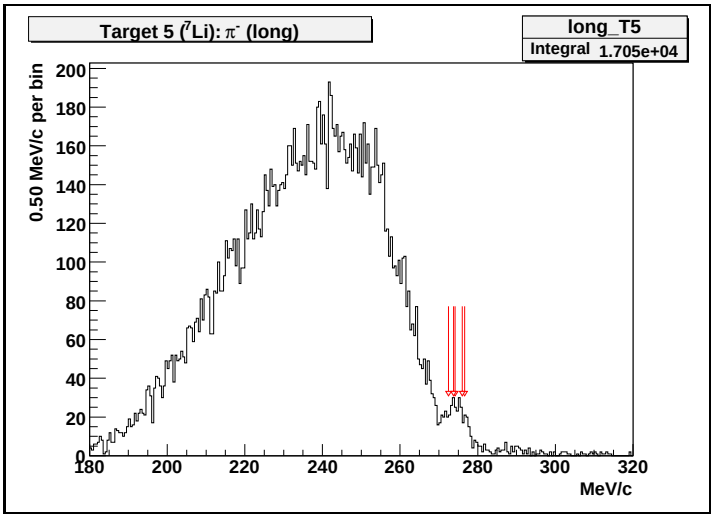

Figure 3.5: π^- inclusive momentum spectrum for events with the K^- stopping in ^{7}Li target n. 5. Long, high resolution (four points) and forward tracks selected.

ing to the expected momenta for the ground and first excited states – some of them are overlapping and cannot be disentangled yet with the present resolution, but a clear indication of the most populated one at 272 MeV/c, which is expected to be produced with a capture rate of about $7 \times 10^{-4}/\mathrm{K}^-_{stop}$, is present in the spectrum. From a single target, about 100 events have been collected in the most populated peak.

The signals out of the deuterated water target are very interesting as well. For the $^{16}_{\Lambda}$O hypernucleus signals are expected in the momentum spectrum at 279.20, 271.50, 267.01 and 260.44 MeV/c. All the four levels are visible in the experimental spectrum, in spite of just one target available. With the events that can be extracted from the ground state peak, interesting coincidence studies can be done on $^{16}_{\Lambda}$O non-mesonic weak decays, and will be described later.

3.3 Hypernuclei Decays

We present in this section some preliminary results concerning the non-mesonic decay mode of several observed hypernuclei. The analyses are still underway, therefore in some cases background subtraction and acceptance corrections are still missing. The job is, of course, in progress.

3.3.1 Non-Mesonic Weak Decays

The $^7_{\Lambda}$Li case

Coincidence events with a proton emitted together with a π^- from the same vertex were searched. The coincidence π^- spectrum, cumulating the statistics collected in the two available ^{7}Li targets, is presented in Fig. 3.6. The signal from the $^7_{\Lambda}$Li g.s. hypernucleus (red region) emerges clearly. The blue area in

the inset corresponds to events in the bound region for the formation of ${}^{5}_{\Lambda}$He, that can also be singled out in this spectrum.

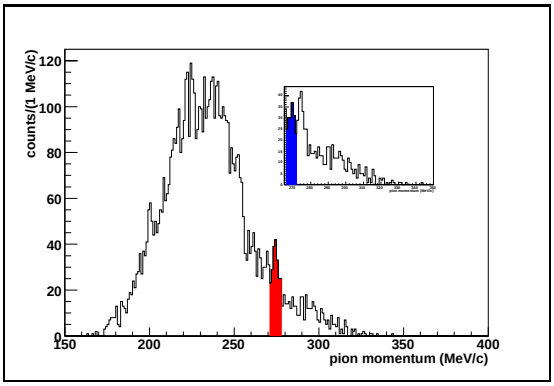

Figure 3.6: π^- spectrum for events with an additional proton track, from the two ^{7}Li targets used in the 2006-2007 data taking. The red area corresponds to the formation of ${}^{7}_{\Lambda}$Li g.s., while the blue one in the inset to the formation of ${}^{5}_{\Lambda}$He.

The events with a π^- in the momentum region for the formation of ${}^{7}_{\Lambda}$Li ground state (199 events) have a proton energy spectrum reported in Fig. 3.7, without acceptance correction. A considerable extension of the spectrum to lower energies, thanks to the thinness of the FINUDA targets, must be remarked as an outstanding feature of our data in comparison to existing first class results for this measurement [4].

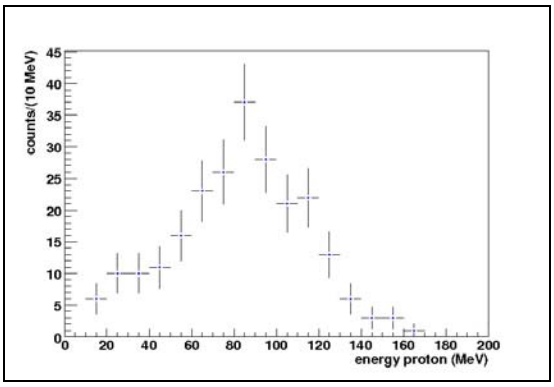

Figure 3.7: Energy spectrum of the protons emitted in coincidence with π^-'s selected in the ground state region for the formation of the ${}^{7}_{\Lambda}$Li hypernucleus, from the two ^{7}Li targets used in the 2006-2007 data taking, *not* acceptance corrected.

Fig. 3.8 shows the proton energy spectrum (not acceptance corrected) for events selected in the blue area of Fig. 3.6, *i.e.* corresponding to the non-mesonic decay of ${}^{5}_{\Lambda}$He.

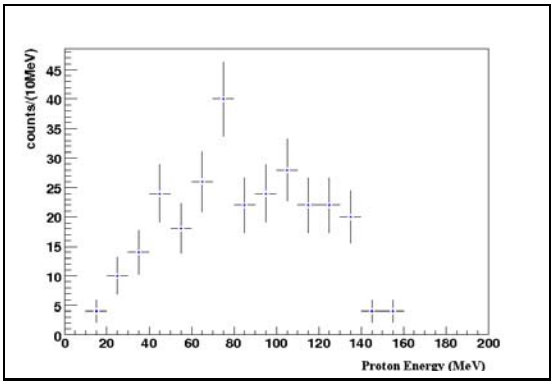

Figure 3.8: Energy spectrum of the protons emitted in coincidence with π^-'s selected in the ground state region for the formation of the ${}^{5}_{\Lambda}$He hypernucleus, from the two ^{7}Li targets used in the 2006-2007 data taking, *not* acceptance corrected. The integral amounts to 202 events.

In the ${}^{7}_{\Lambda}$Li case a reliable background subtraction of the signal can tentatively be performed. Since in the momentum region beyond the bound states only the K^-2N absorption reaction is effective (with the production of Σ^- and its subsequent decay and/or conversion), we can subtract from the momentum spectrum the contribution of this channel normalized to the tail strength. A Montecarlo calculation was performed using, for the K^-2N reaction simulation, the dynamical parameters valid for the well known ^{12}C nucleus [5]. Fig. 3.9 shows the background contribution fitting the π^- momentum tail, as well as the result of the subtraction of the K^-2N contribution from the acceptance corrected proton spectrum.

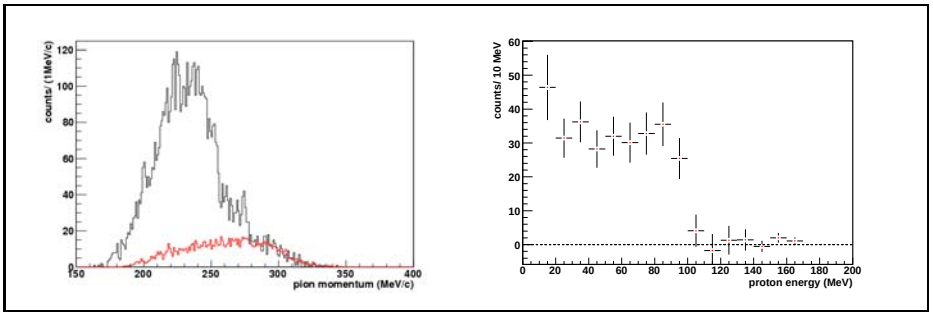

Figure 3.9: Left: π^- spectrum for events with an additional proton track and, superimposed (red histogram), the contribution to the spectrum of the K^-2N channel, normalized to the spectrum tail; Right: proton energy spectrum for ${}^{7}_{\Lambda}$Li ground state events, background subtracted and acceptance corrected.

The expected signal from proton induced non-mesonic weak decay appears between 80 and 100 MeV, together with a rise in the region of lower energies, that can be addressed to Final State Interaction (FSI) effects as well as to two

nucleons induced non-mesonic weak decays. The comparison with the generic FSI shapes predicted by theoretical models (for instance in Ref. [6]) seems to tell us that FSI effects only cannot explain the full appearance of the experimental spectrum. Further studies are of course underway.

With the present data, a first estimation of the branching ratio for proton induced non-mesonic weak decay of the $1s$ level of ${}^{7}_{\Lambda}$Li was attempted: $\Gamma_p = (0.35 \pm 0.10)$ [7].

The ${}^{5}_{\Lambda}$He case

Fig. 3.10 shows the inclusive spectrum of protons out of K^-'s stopping in ^{6}Li, for both the two available targets, not acceptance corrected.

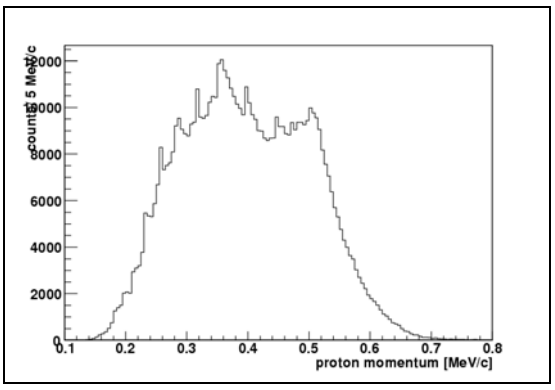

Figure 3.10: Inclusive proton momentum spectrum for events with a K^- stop in one of the two ^{6}Li targets used in the 2006-2007 data taking, not acceptance corrected.

This spectrum can be compared to the one published in Ref. [8], taking however into account a larger population of the low momentum part of the spectrum, due to inclusion of shorter tracks which in the analysis of 2003-2004 data were not reconstructed by the current version of the pattern recognition. In this spectrum the peak at about 505 MeV/c is always present and due to the quasi-free absorption of K^- on two nucleons: $K^-(np) \to \Sigma^- p$; the peak emerging at about 370 MeV/c is due, on the other hand, to the quasi-free reaction $K^- n \to \Lambda\pi^-$. At 235 MeV/c a signal due to fake μ^+ from $K_{\mu 2}$ decays may also be observed. Other spurious dips emerge in the spectrum as a consequence of shadowing effect of some apparatus mechanical supports; they should be healed by the acceptance correction, that is currently in progress as well as a fresh analysis of the $K^-(np) \to \Sigma^- p$ absorption reaction with the new data.

The study of the ${}^{5}_{\Lambda}$He hypernucleus weak decay is feasible since the π^- spectra give indication of the formation of the ${}^{5}_{\Lambda}$He hyperfragment. Summing up the statistics and requiring a proton track emitted from the same vertex one gets the spectrum in Fig. 3.11 where a clear peak can be observed in the bound region for the formation of the ${}^{5}_{\Lambda}$He hypernucleus (red area), which subsequently decays following the non-mesonic mode.

The corresponding proton energy spectrum, without acceptance correction, is shown in Fig. 3.12: the bulk of the signal is located, as expected, around

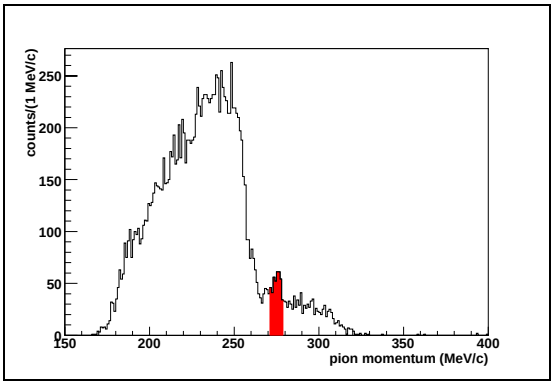

Figure 3.11: π^- spectrum for events with an additional proton track, from the two ^{6}Li targets used in the 2006-2007 data taking.

80–100 MeV. Even in this case the extension of the spectrum down to less than 20 MeV is a remarkable feature that only FINUDA can exploit, thanks to the use of thin targets.

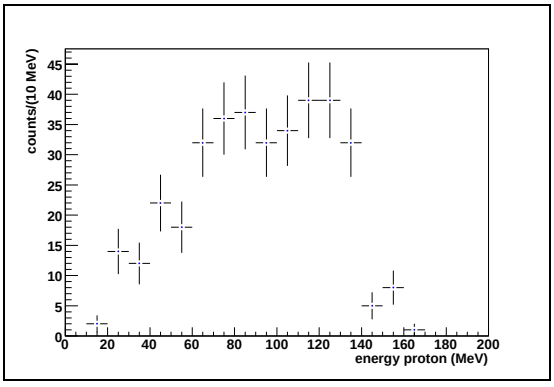

Figure 3.12: Energy spectrum of the protons emitted in coincidence with π^-'s selected in the ground state region for the formation of the $^5_\Lambda$He hyperfragment from the two ^{6}Li targets used in the 2006-2007 data taking. The plot is *not* acceptance corrected.

About 450 events populate the spectrum. It is remarkable to note that this spectrum is fully compatible with the one shown in Fig. 3.8, obtained selecting events with K^- stopping in ^{7}Li targets.

After the acceptance correction one gets the spectrum shown in Fig. 3.13: the region in the 20–40 MeV rises considerably, as a consequence of FSI effects and several multi-nucleon induced processes, among which a sizeable contribution could be given by the non mesonic decay induced by two nucleons [7].

The analysis of background subtraction is currently underway, as it is particularly complex due to the peculiar two-cluster (αd) structure of the ^{6}Li nucleus.

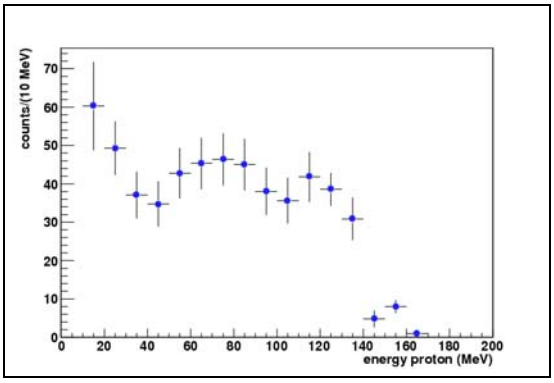

Figure 3.13: Energy spectrum of the protons emitted in coincidence with π^-'s selected in the ground state region for the formation of the ${}^{5}_{\Lambda}$He hyperfragment from the two ^{6}Li targets used in the 2006-2007 data taking, acceptance corrected but not background subtracted.

The ${}^{16}_{\Lambda}$O case

A first observation of the proton induced non-mesonic weak decay of the ${}^{16}_{\Lambda}$O hypernucleus has been made with the new data. Asking both forward and backward π^- long tracks in coincidence with a further proton track emitted from the same vertex one gets the spectrum reported in Fig. 3.14.

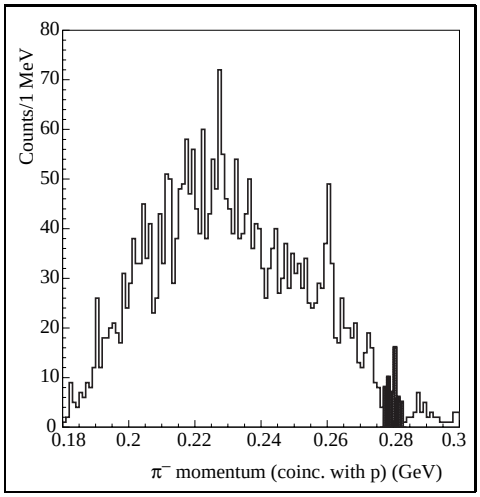

Figure 3.14: π^- momentum spectrum for events with an additional (long) proton track emitted from the D_2O target. The black area corresponds to the formation of the ground state ${}^{16}_{\Lambda}$O hypernuclei.

Here the peak of the ${}^{16}_{\Lambda}$O g.s. hypernucleus is evident in the $(277 \div 289)$ MeV/c region (black area in the histogram). The energy spectrum of the protons for the events selected in the ground state region (about 70) is shown in Fig.

3.15, before the acceptance correction.

The spectrum shows basically the same features observed in the two previous cases, namely a broad peak at about 80 MeV clearly providing the signature of a proton induced non-mesonic weak decay.

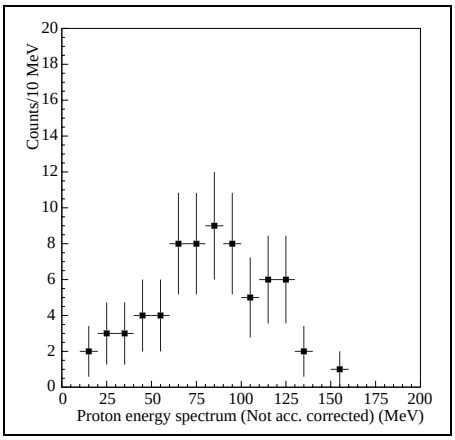

Figure 3.15: Energy spectrum for protons emitted in coincidence with the formation π^- of the ${}^{16}_{\Lambda}$O hypernucleus, without acceptance corrections.

Fig. 3.16 shows the same spectrum after the acceptance correction.

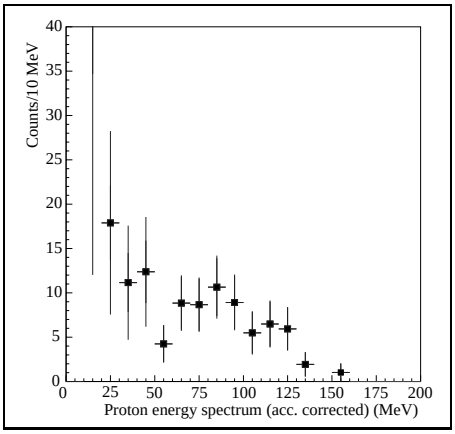

Figure 3.16: Energy spectrum for protons emitted in coincidence with the formation π^- of the ${}^{16}_{\Lambda}$O hypernucleus, after acceptance corrections.

Study of the background subtraction is in progress, but it is not expected to be relevant in this case.

3.3.2 Rare decays: ${}^{4}_{\Lambda}\mathrm{He} \rightarrow d + d$

As reported in larger detail in the following (see Sec. 3.5.1) with the present amount of data a closer search for events with two "monochromatic" deuterons coming from the decay of the ${}^{4}_{\Lambda}$He hyperfragment can be performed. This hypernucleus is produced as an hyperfragment from virtually every target, even if a more abundant production is expected in case of a K^- interacting with lighter nuclei. The signature of its decay, occurring at rest, is a deuteron pair, back-to-back emitted, with a momentum of 570 MeV/c each.

By means of a *p.id.* identification of the two deuterons using the energy loss response of OSIM and the LMDC's and the information of the TOF we are able to identify about 45 deuteron pairs, whose relative angle distribution is shown in Fig. 3.17.

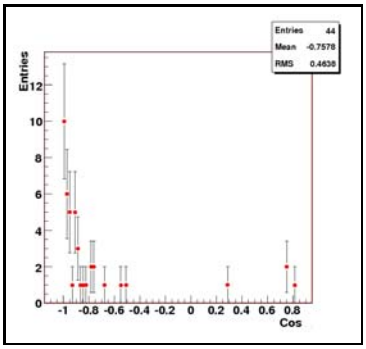

Figure 3.17: Angle between two deuterons identified as emitted from the same vertex, in all targets.

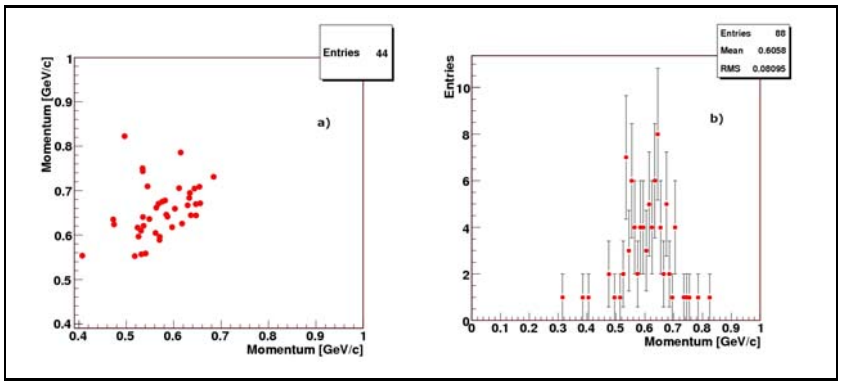

Figure 3.18: Left (a): Scatter plot of the momenta of the two deuterons identified in each event in the search of ${}^{4}_{\Lambda}\mathrm{He} \rightarrow d + d$ decay; Right (b): one-dimensional distribution of the deuteron momenta, two entries per event.

The figure shows a marked back-to-back correlation, for tracks whose momenta are distributed according to the scatter plot shown in Fig. 3.18a). In Fig. 3.18b) the cumulative distribution of the deuteron momenta is reported

(two entries per event).

From the scatter plot a systematic correlation of high-low momentum tracks can be deduced: a "higher" momentum deuteron is always associated to a "lower" momentum one. This is a known feature of the data and can be easily explained reminding that backward tracks have to cross the whole inner region (ISIM, TOFINO, beam pipe) before being tracked in the opposite emisphere; therefore the momentum of the particle must be carefully corrected taking into account the energy lost in the crossing of each of the volumes. The correction procedure is currently under completion and can be considered as a sort of "offline" additional calibration of the data [9]. A first rough estimate provides, for this channel, a decay rate per K^- stop of the order of 10^{-5}.

We recall that, with the same analysis procedure, in the first data taking just three complete $d + d$ events were identified, therefore the improvement of data quality and apparatus performance concerning its *p.id.* capabilities and the precision of the TOF calibrations is evident.

3.4 Neutron Rich Hypernuclei Searches

Fig. 3.19 shows the "signature" we had in our first data taking for the signals of ${}^{6}_{\Lambda}$H and ${}^{7}_{\Lambda}$H in the corresponding Region Of Interest (ROI in the following), from ^{6}Li and ^{7}Li targets respectively [10].

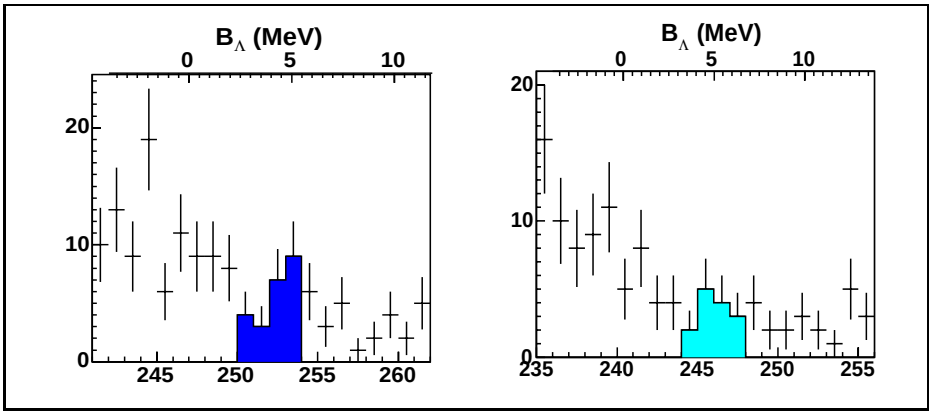

Figure 3.19: π^+ momentum spectrum in the region interesting for the search of ${}^{6}_{\Lambda}$H and ${}^{7}_{\Lambda}$H from ^{6}Li (left) and ^{7}Li (right) targets, 2003-2004 data taking [10]. The coloured areas correspond to the events in the ROI for the formation of the mentioned Neutron Rich hypernuclei.

For the search of Neutron Rich Hypernuclei a good identification of the positive pions must be achieved. With a large statistics more stringent cuts as compared to the previous data taking can be applied, selecting long, well fitted and high resolution (four-point) forward tracks. On $\sim$ 1 MeV/c resolution selected tracks the particle identification can be made using the information of the energy loss from the OSIM modules as well as from both the drift chamber arrays, in order to select minimum ionizing particles against protons. Moreover, information from TOF can be used as well to the same purpose.

The basic problem is represented by a feed-through of positive muons from K^+ decays due to an incorrect K^+/K^- vertex assignment. Ways to recover the wrong $K^\pm$ vertex assignment are currently under development; at the moment, a set of cuts involving the ϕ and K^- vertex coordinates have been identified, which reduce considerably the contamination from fake events. They basically take into account the larger algorithm inefficiency for some topological configurations of the K^+/K^- helices, and consist of a tighter selection on the ϕ vertex coordinates, which reduces the overall contamination of about 4%.

A further selection asking for the coincidence of a μ^+ coming from a K^+ decay doesn't help very much, on the contrary, to reduce the contamination from fake events – the statistics are reduced of a factor about 10, but no improvement is observed in the quality of the signals in the ROI.

In the following a preliminary overview of the π^+ spectra obtained with the cuts on the ϕ vertex coordinates is reported.

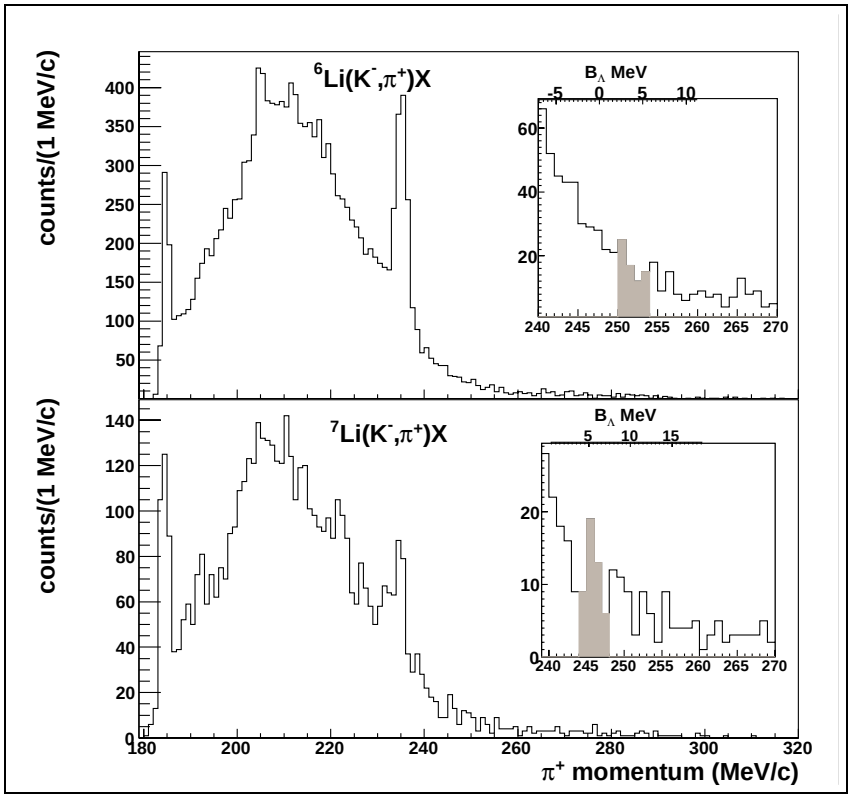

Figure 3.20: π^+ momentum spectrum from ^{6}Li (top) and ^{7}Li (bottom) targets. The grey areas in the insets, which zoom the final part of the spectra, correspond to the events in the Region Of Interest for the formation of Neutron Rich Hypernuclei.

The available events in the ROI for the formation of Neutron Rich Hypernuclei are evidenced in grey in each inset in the Figures. The most interesting signal come from both from ^{6}Li and ^{7}Li targets, shown in Fig. 3.20: in the new data taking 67 and 49 events are collected, respectively, in the ROI, to be

compared with 7 and 2 events observed with the data of the first FINUDA run by appliying the same cuts and reconstruction procedure (tighter than those used in Ref. [10]): a tenfold statistics is gained.

An interesting signal seems to emerge especially from the ^{7}Li targets. A finer tuning on alignments will probably help to single out better this peak.

Less clear signals emerge from the other targets. In Fig. 3.21 the π^{+} spectra for events from ^{9}Be, ^{13}C and ^{16}O are shown:

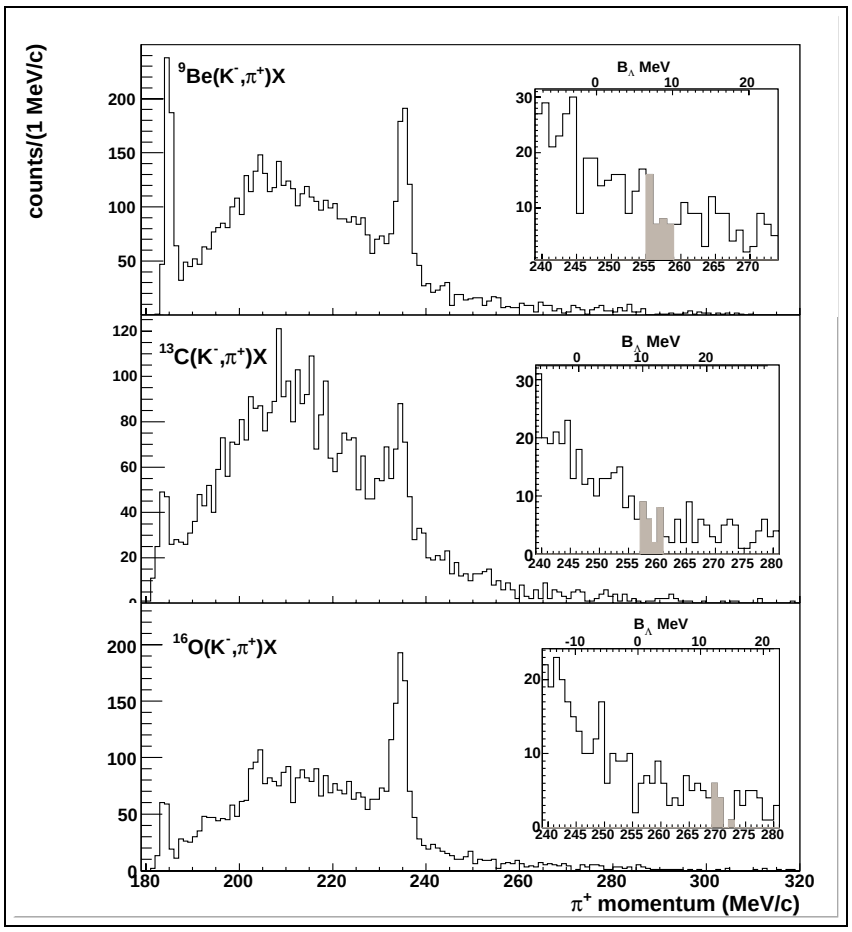

Figure 3.21: π^{+} momentum spectrum from ^{9}Be (top), ^{13}C (center) and ^{16}O (bottom) targets. The grey areas in the insets, which zoom the final part of the spectra, correspond to the events in the Region Of Interest for the formation of Neutron Rich hypernuclei.

3.5 Deeply Bound Kaon Nuclear States

The amount of statistics collected in the last data taking is good enough to allow accurate studies of possible Λp and Λd states in different targets, in order to understand medium dependent effects which could be ascribed to FSI. In

the following a short discussion of the FINUDA improved capability in the identification of particles will be given, followed by a first survey of the $(\pi^- p)p$ and Λd signals that can be observed in different targets.

3.5.1 Particles identification

Λ identification

Fig. 3.22 shows the invariant mass of the $(\pi^- p)$ system (K^- vertex in any target), which gives a clear signal corresponding to the Λ peak. The black histogram corresponds to events selected by applying the standard cuts (π^- and protons identified by means of the energy loss in the three layers of the tracker, well fitted tracks reconstructed with a minimum of three points). A further cut was then applied asking for the presence of a secondary vertex: in the last months, in addition to the new version of the pattern recognition which allows the reconstruction of tracks with less than four points in the spectrometer, a new secondary vertex search algorithm was in fact developed to help the identification of two- and many-body decaying particles, through their decay topology. The red histogram in Fig. 3.22 shows the effect of a cut of this type: the background contribution is heavily reduced.

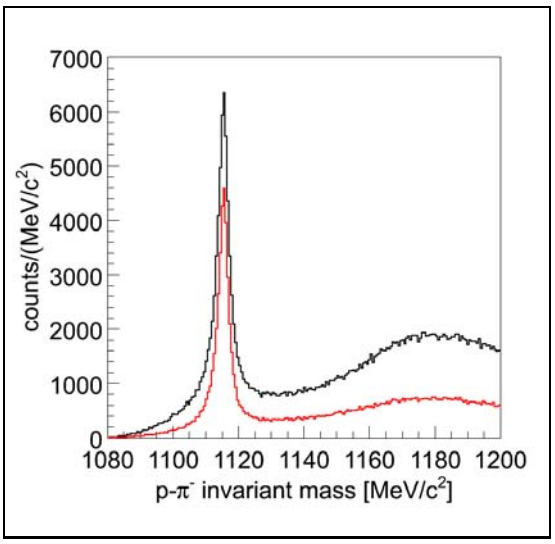

Figure 3.22: $\pi^- p$ invariant mass for events with a K^- vertex in any target. The black histogram corresponds to event selected with standard quality cuts for tracks (see text); in the red one events in which a secondary vertex was found were selected.

Indeed, the distance between the K^- stop vertex in the target and the secondary vertex (obtained by the track crossing in the apparatus) is a powerful tool to increase the signal/noise (S/N) ratio.

A study of the S/N ratio for the Λ signal was performed target by target, in order to understand the effect of the single cuts applied for the selection of π^- and p tracks and of the secondary vertex. For instance, Fig. 3.23 shows

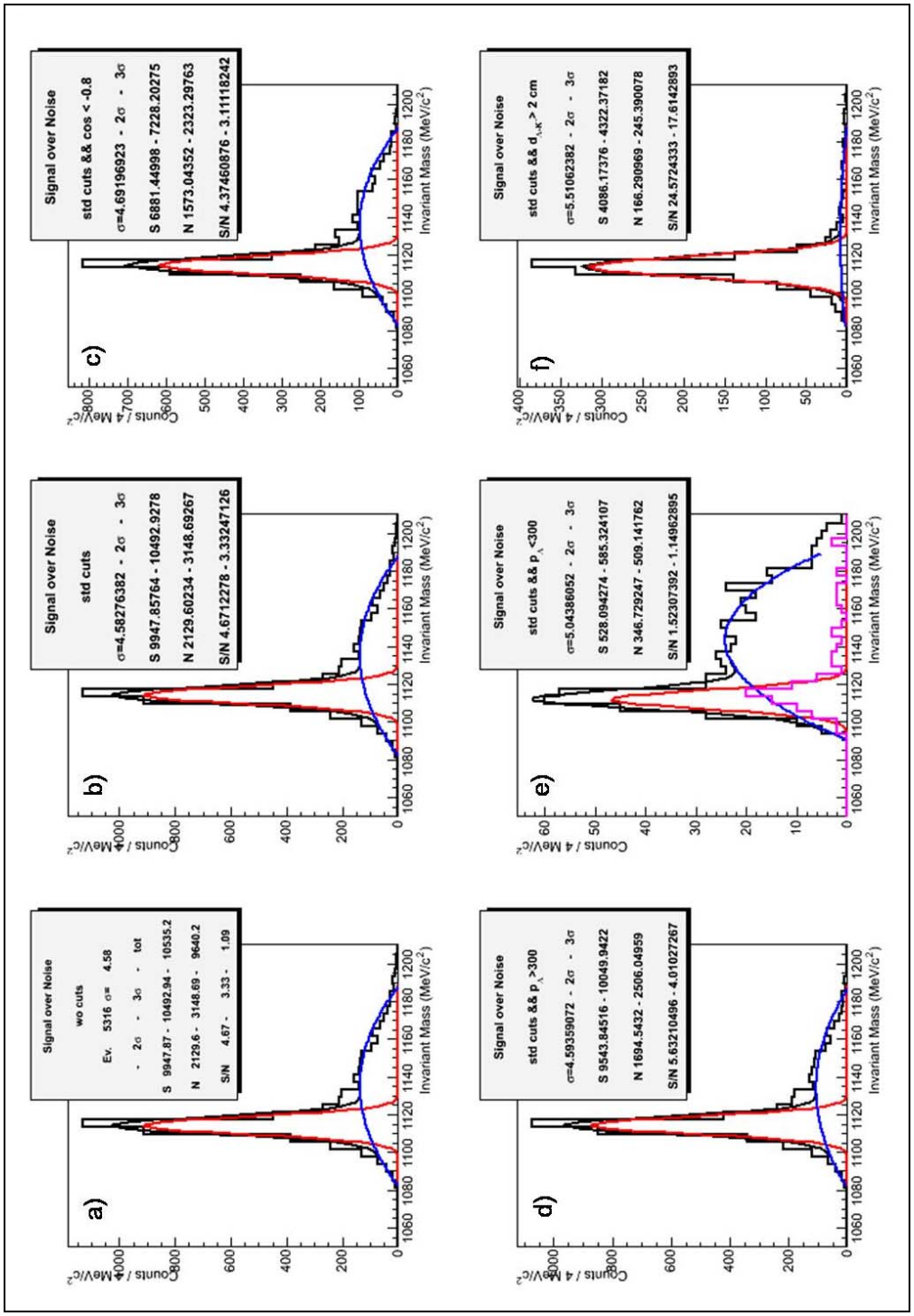

Figure 3.23: $(\pi^- p)$ invariant mass for events with a K^- vertex in ^{6}Li targets. The plots differ for the sets of cuts applied for the track selection: upper left a): no cuts; upper center b): standard track cuts (well fitted tracks reconstructed with at least three points, π^- and protons identified by means of dE/dx in the three layers of the tracker); upper right c): standard cuts and back-to-back angular cut; lower left d): standard cuts and Λ momentum larger than 300 MeV/c; lower center e): standard cuts and Λ momentum lower than 300 MeV/c; lower right f): standard cuts and distance between K^- stop vertex and secondary vertex larger than 2 cm. Red lines: signal, Blue lines: background.

the quality of the Λ signal obtained from tracks emitted from ^{6}Li targets when passing through different sets of cuts.

The description of the applied cuts is reported in the figure caption. It is clear how the secondary vertex requirement improves considerably the S/N ratio: with standard track cuts the ratio, at 2σ, is 3.3 (upper center plot b)); requiring an additional cut on back-to-back tracks (upper right plot c)) the S/N ratio reduces to 3.1: the back-to-back cut is in general rather scarcely effective due to the particular topology of the accepted events. Then, applying a cut on the impact parameter with the requirement of the secondary vertex to be located more than 2 cm away from the K^- stop point in the target, the S/N ratio at 2σ rises to $\sim$ 18 (f). The same happens for the other targets, with an improvement of the S/N ratio of a factor 4 to 6 when applying cuts involving the secondary vertex topology.

The new pattern recognition helps considerably in extending the acceptance for the Λ, allowing to measure low momentum particles ($140 < p_\Lambda < 300$ MeV/c) which otherwise, requiring "long" tracks only, would have been missed (as it was in our first analysis [11], in which Λ's slower than 300 MeV/c were out of the reconstruction acceptance.) Fig. 3.24 shows, on the left, a scatter-plot of the invariant mass of the $(\pi^- p)$ system vs the total momentum: a long stripe, corresponding to the Λ invariant mass, extends in the momentum range (100 $\div$ 700) MeV/c, showing the larger momentum acceptance that can be achieved with the new reconstruction algorithm. Requiring long tracks only, the stripe started at just 250 MeV/c. In the same plot, a sizeable signal most probably from Δ^0 is visible, as a blob centered about 1200 MeV/c^2.

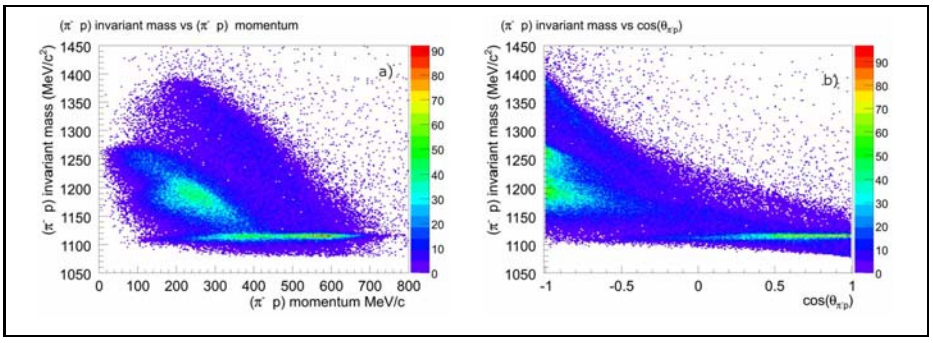

Figure 3.24: Left (a): $(\pi^- p)$ invariant mass vs $(\pi^- p)$ measured momentum: the signals from Λ and Δ formation are clearly visible. Right (b): $(\pi^- p)$ invariant mass vs $\cos(\pi^- p)$.

Also the angular correlation of the two tracks for events selected in the Λ stripe shows an increase of the opening angle acceptance. This is shown in the right picture of Fig. 3.24, a scatter plot of the $(\pi^- p)$ invariant mass vs their relative angle. It appears clearly from the Figure that decays at rather large angles ($\cos(\pi^- p)$ down to -0.5) can be detected, to be compared with the very forward tracks ($\cos(\pi^- p) > 0.25$) filtered in the analysis with long tracks only.

d and heavier particles identification

In FINUDA the particle identification may be performed by means of the specific ionization energy loss, and/or by time of flight measurements. Fig. 3.25 the energy loss response from two sensible layers of the FINUDA apparatus is shown, versus the momentum of the track measured in the apparatus: on the left, the dE/dx measured by OSIM, on the right, the dE/dx measured in one of the two LMDC's layers (namely, the inner one).

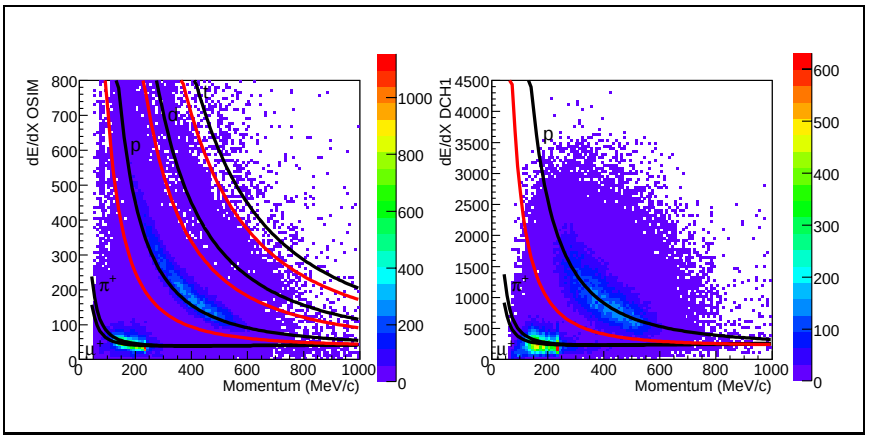

Figure 3.25: Specific energy loss response vs the tracks momentum as measured in the apparatus by two of the FINUDA sensible detectors: left: dE/dx measured in OSIM; right: dE/dx measured in the inner LMD's. The red lines represent the limits of the bands chosen for particle identification.

The responses of the detectors to the specific ionization have the classical Bethe-Block shape upon which proper bands (red lines) centered on the expected curve for each particle can be drawn in order to identify the particles. While the LMD's are mainly useful to separate *m.i.p.*'s from the rest, the vertex detectors layers can be effectively used to select proton, deuterons and possibly heavier particles like tritons. Coupling the information on energy loss from different ionization detectors the efficiency for proton identification is higher than 96%.

The addition of information of the β of the track coming from TOF measurement can help further to identify with good confidence and small contamination the presence of heavier particles. In Fig. 3.26, where the $1/\beta$ vs track momentum is shown, the magenta points represent events compatible with a triton (or heavier nucleus) assignment by the TOF measurement (and recognized as deuterons or heavier particles by dE/dx on OSIM and LMDC's). Quite surprisingly we see an unexpected number of such heavy particles: the physical processes responsible for such a production are currently under study.

The $1/\beta$ picture shows clearly the quality of TOF system calibration: the main gatherings are located exactly along the black lines corresponding to the expected velocity for (from bottom to top) *m.i.p.*'s, protons, deuterons, tritons and possibly heavier particles, which can be measured with enough confidence if their momentum is larger than ~ 500 MeV/c.

Fig. 3.27 shows in detail the usefulness of TOF information for the selection

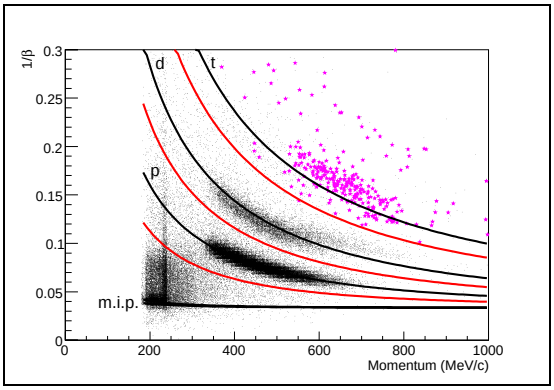

Figure 3.26: $1/\beta$ vs track momentum as measured by the FINUDA Time Of Flight system. The magenta points mark the events recognized as tritons or heavier particles by the β measurement, and by deuterons or heavier particles by dE/dx in OSIM and LMDC's. The black lines represent the expected velocity vs momentum relationship for several particles, while the red lines represent the limits of the bands used for their identification.

of heavy ionizing particles. The plot is the particle mass derived by the β and momentum information, for events with a specific energy loss compatible with a deuteron (or heavier particle) one as measured by both ISIM/OSIM and LMD's layers (blue left-hatched histogram).

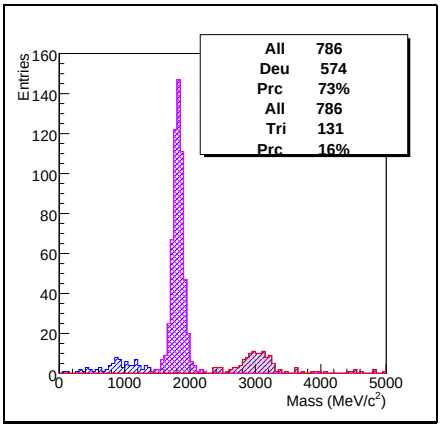

Figure 3.27: Mass distribution, obtained from dE/dx, β and momentum information, for particles heavier than protons. Blue left-hatched histogram: tracks selected as deuterons or heavier particles by means of dE/dx by both OSIM and LMD's layers. Magenta right-hatched and red-dotted histograms: deuterons and tritons, respectively, selected by TOF only.

A small contamination from proton events feeds through in the distribution. The events whose β is compatible with a deuteron are collected in the magenta right-hatched histogram: the compatibility with the dE/dx response is complete. On the other hand, a small accumulation of events at higher mass, about 3 GeV/c^2, is compatible with a time of flight typical of a triton (red dotted histogram). These events, at the moment, are identified as deuterons by the energy loss measurement in ISIM/OSIM: a finer charge calibration aimed to recover a correct identification of these events (not foreseen in the detector design) is currently underway.

This information gives a promising hint for a possible future search of Λt aggregates, at least for tritons with momenta higher than 500 MeV/c.

3.5.2 $(\pi^- p)p$ events and invariant mass spectra

The first paper published by FINUDA on the evidence of a Deeply Bound K$^-$-Nuclear States (DBKS in the following) observed in the $(K^- pp)$ system [11], riding the tide of the first observations in agreement wih Akaishi-Yamazaki (A-Y) model [12], needs an urgent confirmation with the data collected recently, as in the following years several criticisms raised.

On the experimental point of view, the first claims [13] were recently withdrawn [14] –and, moreover, FINUDA itself showed that signals observed in a similar way in inclusive spectra have a thoroughly simple explanation without resorting to exotic interpretations [8]. On the theoretical point of view, apart from several open criticisms to the A-Y model, the FINUDA result [11] was criticized in that it was claimed that the data could to be simply explained by FSI effects [15]. Even if the dominant role of FSI can be already questioned by indirect observations (namely, by the study of the proton spectra emitted in the non mesonic weak decay of $^{12}_{\Lambda}$C [5], see also par. 3.3.1 of this report), a convincing tool to disprove this interpretation would be the observation of the same signal in different targets, where the FSI effect should act differently, more sizeably in heavier nuclear media.

For this reason a new analysis was soon started on the freshly collected data, following basically the same exclusive approach as in Ref. [11], now target by target. At the same time, the problem was also attacked in a different way (resorting to inclusive spectra), in order to cross-check possible biasing effects.

Λp exclusive analysis

Fig. 3.28 shows a comparison between the analysis published in Ref. [11] and the new data, selected according to the same criteria and according to the target where the K^- stops.

We recall that in this analysis long (four points reconstructed) proton tracks, a pion track reconstructed with at least three points and Λ identification were required; then an angular cut between the selected Λ and the recoiling proton was applied, asking for a back-to-back correlation. The amount of events entering the invariant mass (Λp) spectrum was about 200, cumulating the events with the K^- stop point in ^{6}Li, ^{7}Li, and ^{12}C targets (6 targets overall). Fig. 3.28a) shows the spectrum obtained with 2003-2004 data, not corrected for acceptance. This spectrum has to be compared to what we get in the 2006-2007 data taking from each target (further analysis currently underway [16]): b) ^{6}Li (356 events),

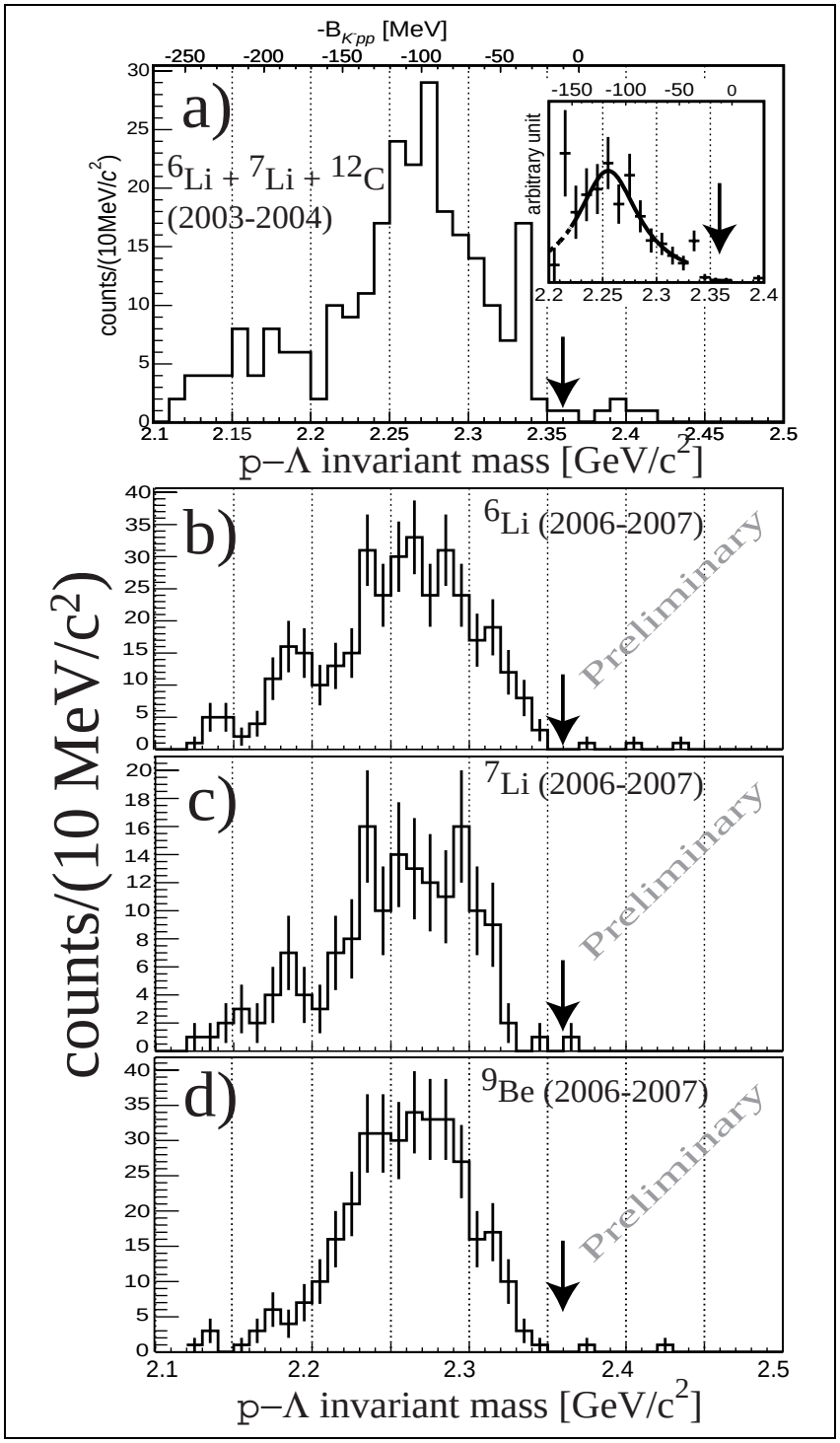

Figure 3.28: Acceptance not-corrected (Λp) invariant mass distributions for: a) 2003-2004 data, all light targets ($2\times^6$Li, $1\times^7$Li and $3\times$ 12C) (in the inset the acceptance corrected and fitted spectrum is shown [11]); b) 2006-2007 data, $2\times^6$Li targets; c) 2006-2007 data, $2\times^7$Li targets; d) 2006-2007 data, $2\times^9$Be targets. The arrows mark the (K^-pp) threshold.

c) ^{7}Li (157 events), d) ^{9}Be (340 events). The shape of the spectra, though not corrected for acceptance yet, is similar enough to indicate a probably common mechanism effective in all targets to produce an aggregate at a mass lower than the $(K^{-}pp)$ threshold (indicated in the Figure with arrows).

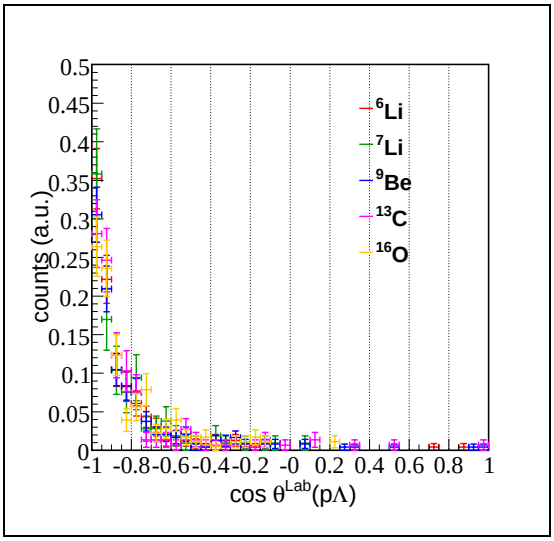

Figure 3.29: Distribution of the angle between a Λ and a proton emitted in coincidence from different targets: ^{16}O (yellow histogram), ^{13}C (magenta), ^{9}Be (blue), ^{7}Li (green), ^{6}Li (red). Not acceptance corrected.

A first interesting hint concerning the contribution of FSI's can moreover be observed in the trend of the angular distribution between the selected Λ and the recoiling proton, in different targets. We recall that in our first publication [11] a marked back-to-back correlation was found, but no dependence on the target could be traced due to the scarcity of the available statistics (for this reason the distribution shape was prone to the interpretation of being simply due to FSI [15]). It is possible now to study the angular distribution from different targets, reported in Fig. 3.29.

No significant difference between the distributions can be observed at this stage of the analysis, that could point to the dominance of FSI effects which should behave differently according to the weight of the nuclear target inside which the interactions occur.

$(\pi^{-}p)p$ inclusive analysis

The exclusive analysis method has as drawback the fact that one could possibly bias the result by forcing cuts which might constrain a defined region of the phase space available for the reaction.

In this spirit, a new approach was attempted relying on very loose initial cuts leading to inclusive spectra, and then applying gradually further selections when correlated information emerge from them. To this purpose it is clear that good statistics are necessary in order to extract the signal features and to reduce at the same time the possible background sources, and this can be done with the

new data at our disposal. A preliminary analysis on the old data following this method was indeed previously pursued, leading to results compatible with the published ones, even if a sizeable background subtraction had to be applied to extract the physical signal since due to the limited statistics a reduced number of cuts could be made [17].

The first rough selection requires simply the identification of the three particles with a momentum of the $(\pi^- p)$ system larger than 140 MeV/c, and the momentum of the recoiling proton larger than 180 MeV/c. Given three well identified particles per event, several scatter plots can be made and one of the most interesting is the correlation between the invariant mass of the $(\pi^- pp)$ system and the angle formed between the $(\pi^- p)$ pair and the recoiling proton. The plot is shown in Fig. 3.30, for events with K^- stopping in the ^{6}Li targets. A clustering can be noted for back-to-back opening angles, with a dominant contribution around 2200 MeV/c^2 and a second gathering between 2250 and 2300 MeV/c^2.

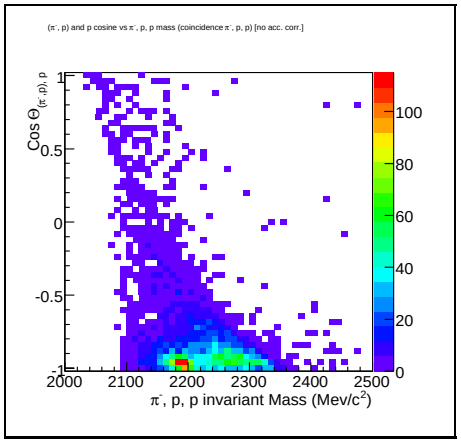

Figure 3.30: Scatter plot of the invariant mass of the $(\pi^- pp)$ system and the cosine of the angle between a $(\pi^- p)$ pair and the recoiling p, *not* acceptance corrected. Events with K^- stopping in ^{6}Li targets, two entries per event.

If we further require the $(\pi^- p)$ pair in the mass window of the Λ baryon we get the plot in Fig. 3.31 (left), where now a strong correlation between back-to-back Λ and p can be inferred when the (Λp) system has a mass in the second of the two intervals mentioned above.

Further cuts (among which the most relevant is on the Λ impact parameter) can then be applied to help extracting this "signal" from the background. In the right part of Fig. 3.31 the scatter plot of the cosine of the angle between a Λ and a p and the invariant mass of the (Λp) system when the impact parameter selection is applied is reported: the region of the "signal" is enhanced while the background is largely reduced.

The same effect can be seen also in ^{7}Li and ^{9}Be targets. In Fig. 3.32a) the (Λp) invariant mass projection of the previous scatter plot with the further requirement of $\cos(\Lambda p) < -0.8$ is shown (acceptance corrected): a bump clearly emerges similar to the one reported in Fig. 3.28b); the low energy tail is due to the acceptance correction. Fig. 3.32b) and 3.32c) report the analogous spectrum

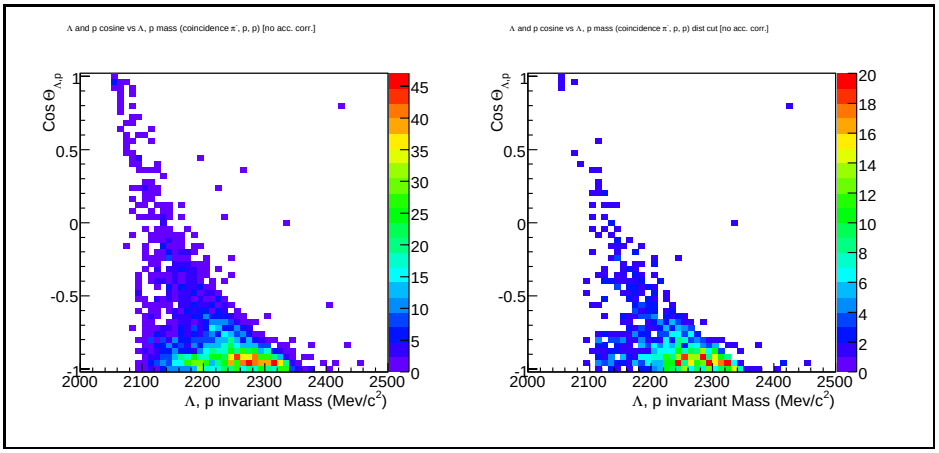

Figure 3.31: Left: Scatter plot of the cosine of the angle between a Λ and a p vs the invariant mass of the (Λp) system, *not* acceptance corrected. Right: Scatter plot of the cosine of the angle between a Λ and a p and the invariant mass of the (Λp) system, with a further requirement on the Λ impact parameter (> 2 cm), *not* acceptance corrected. Events with K^- stopping in ^{6}Li targets.

obtained with the same criteria for ^{7}Li and ^{9}Be, again confirming what shown in Fig. 3.28c) and d), respectively.

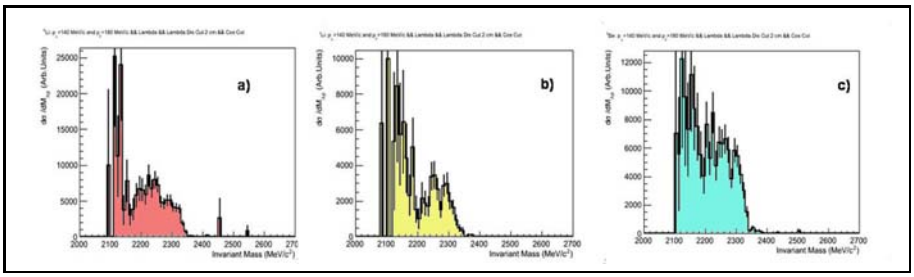

Figure 3.32: a) Invariant mass distribution of the (Λp) system for the ^{6}Li targets, acceptance corrected, obtained from the scatter plot of Fig. 3.31 (right) with the further requirement of $\cos(\Lambda p) < -0.8$; b) same for ^{7}Li targets; c) same for ^{9}Be targets.

These observations make us confident that the obtained results are genuine signatures of a kaon-nuclear bound system, not generated by a phase space artificial distortion. Further work is in progress to finalize quantitatively these analyses.

3.5.3 $(\pi^- p)d$ events and Λd invariant mass spectra

Quite recently a new FINUDA paper was published [18] in which the invariant mass spectrum of the (Λd) system following the capture of K^-_{stop} in ^{6}Li and ^{12}C nuclei was shown: a seemingly "bound" structure could be seen in the case of

^{6}Li. The presence of such a system produced in light nuclei would be a nice confirmation of a genuine bond, since in this case the FSI contribution should be largely reduced as compared to systems decaying in nucleons. With the new data we try to pursue, with many more statistics, the same result in order to confirm our first observation.

The invariant mass spectrum of the $(\pi^- p)$ system recoiling against a deuteron, for events with a K^- stopping in both the ^{6}Li targets, is reported in Fig. 3.33: on the left side, the spectrum obtained in 2003-2004 data taking [18], on the right side the one we get with the new data. The Λ peak emerges clearly with a statistics about 8 times larger.

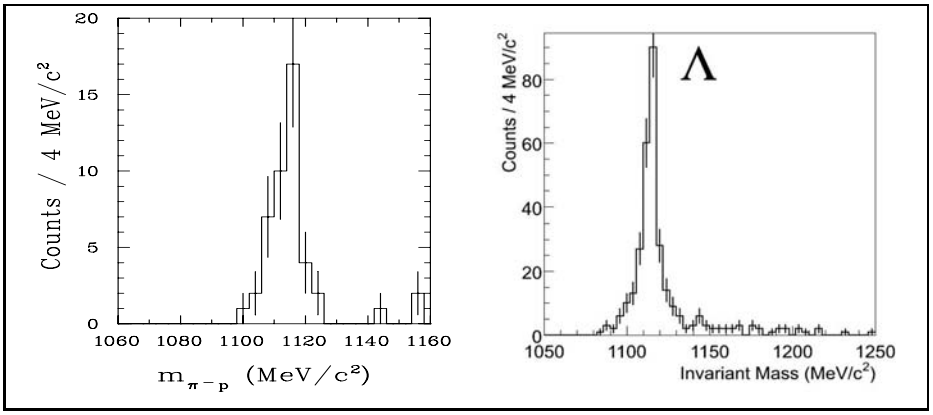

Figure 3.33: Invariant mass of the $(\pi^- p)$ system recoiling against a deuteron for events with a K^- stopping in the two available ^{6}Li targets: left, 2003-2004 data; right: 2006-2007 data.

Again for the sake of comparison, Fig. 3.34 shows the Λd signal obtained with the data of the previous data taking, from the two available ^{6}Li targets.

The plot on the right (b) is what we get from the Λd invariant mass spectrum after acceptance correction: the enhancement on the right part of the spectrum was interpreted as due to a K^--nuclear aggregate with a mass of 3125 MeV/c^2 and a width $\Gamma = 37$ MeV, recoiling against a (nd) pair, in which the deuteron plays as a spectator and the neutron carries away all the excess kinetic energy.

Fig. 3.35 shows the analogous spectra, before and after acceptance correction, obtained from the two ^{6}Li target in the new data taking.

The blue superimposed histogram is obtained by requiring a further back-to-back constraint on the Λ and d emission direction. The present available statistics allows to ask for this further selection that couldn't be applied to the data of the first run, where anyhow a rather marked back-to-back correlation was put in evidence in the study of the signal and its side bands. Fig. 3.35b) shows that the enhancement on the right part of the spectrum survives, still separated from the left part, and the back-to-back constraint helps to single out the signal.

From heavier targets the signal emerges from the raw (acceptance uncorrected) spectra, but its signature, after the acceptance correction, is broader than what is observed in ^{6}Li, in agreement with its absence in the ^{12}C data of

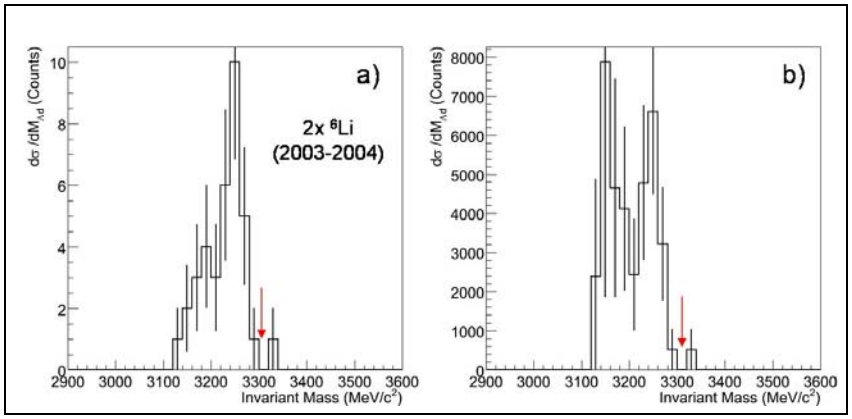

Figure 3.34: Invariant mass of the (Λd) system for events with a K^- stopping in the two available ^{6}Li targets, 2003-2004 data. The plot on the right (b) is obtained by the one on the left (a) after acceptance correction. The red arrow marks the threshold for the $K^- ppn$ quasi-free production.

2003-2004 [18], that is probably due to the dominant FSI contribution in systems with many nucleons. This can be seen, for instance, in the (Λd) invariant mass distribution from the ^{9}Be targets, shown in Fig. 3.36.

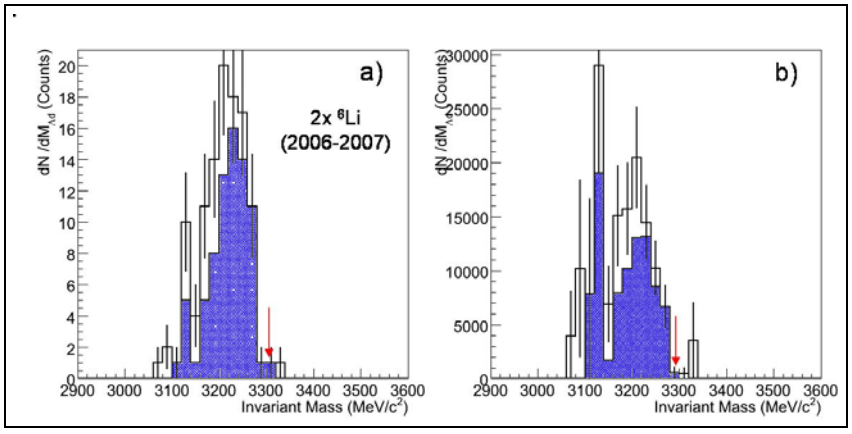

Figure 3.35: Invariant mass of the (Λd) system for events with a K^- stopping in the two available ^{6}Li targets, 2006-2007 data. The plot on the right (b) is obtained by the one on the left (a) after acceptance correction. The blue histogram is what we get requiring a back-to-back correlation between the Λ and the deuteron. The red arrow marks the threshold for the $(K^- ppn)$ quasi-free production.

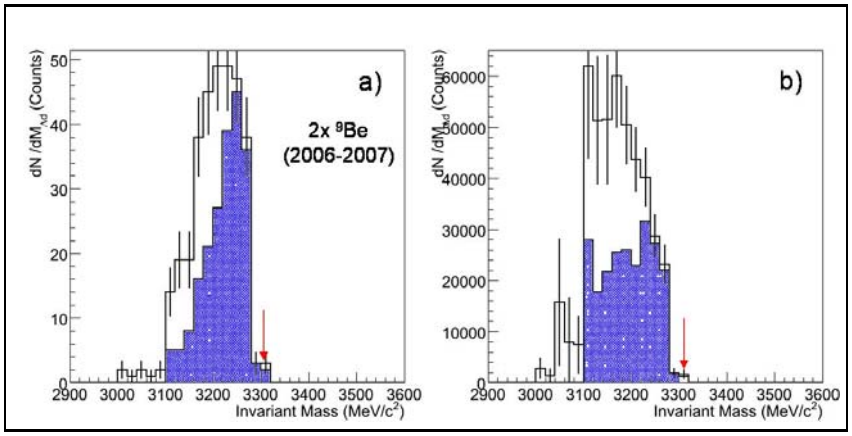

Figure 3.36: Invariant mass of the (Λd) system for events with a K^- stopping in the two available ^{9}Be targets, 2006-2007 data. The plot on the right (b) is obtained by the one on the left (a) after acceptance correction. The blue histogram is what we get requiring a back-to-back correlation between the Λ and the deuteron. The red arrow marks the threshold for the $(K^- ppn)$ quasi-free production.

Chapter 4

Conclusions and Prospects

As of the end of October 2007 a good number of physics analyses have been started and are currently underway: in this report the present status has been summarized.

Service activities are programmed for the last part of 2007 - beginning 2008, including the final fine module alignments, vertex modules charge calibrations, final tuning of time of flight calibrations for critical run groups. When the final tuning will be achieved, the analyses will be repeated on the new calibrated data in a short time since the tools have already been developed and the selection cuts already optimized.

The first round of analysis of the collected data shows an overall good quality, although with a still limited resolution in the range (0.75-0.80)%, which however seems to be affected just very slightly by the He bag air contamination which occurred during the data taking.

The available statistics, as expected, is a factor 6–8 larger with respect to the previous data taking, depending on the studied channel. Moreover, we can now thoroughly base the analyses on a new and extensively tested pattern recognition procedure which helps extending the apparatus acceptance to lower momentum/shorter tracks as well as tracks with missing hits (due mainly to detector inefficiencies). Therefore a large part of events can be recovered.

Moreover, a new algorithm was developed for the identification of secondary vertices, quite helpful in the selection of Λ particles for the search of Deeply Bound K-Nuclear States.

With all the above mentioned improvements in analysis tools and statistics it looks like we are able to confirm the published results on $(K^- pp)$ and $(K^- ppn)$ aggregates.

With the capability of FINUDA (however not foreseen in its design) to identify heavy particles, like deuterons but also tritons at least of high momenta, a possible search of never explored (Λt) correlated pairs could be realistically one of the tasks to be considered if a larger integrated luminosity will be provided in the future to the experiment.

Bibliography

[1] FINUDA Collaboration, *Status Report on FINUDA Data Taking*, February 27, 2007

[2] G. Bonomi in HYP06 Conference (Mainz, October 2006), to be published in the Conference Procedings

[3] The FINUDA Offline Group, *Plans for the next data taking*, November 3, 2006

[4] S. Okada *et al.*, *Phys. Lett.* **B597** (2004), 249

[5] M Agnello *et al.*, *Eur. Phys. J.* **A 33** (2007), 251

[6] E. Bauer, A. Ramos *et al.*, nucl-th/0602066

[7] This work is part of the PhD Thesis of S. Bufalino, University of Torino

[8] FINUDA Collaboration, M. Agnello *et al.*, *Nucl. Phys.* **775** (2006), 35

[9] This work is part of the graduation thesis of S. Baratta, University of Torino

[10] M. Agnello *et al.*, *Phys. Lett.* **B640** (2006), 145

[11] FINUDA Collaboration, M. Agnello *et al.*, *Phys. Rev. Lett.* **94** (2005), 212303

[12] Y. Akaishi and T. Yamazaki, *Phys. Rev.* **C65** (2002), 044005; T. Yamazaki and Y. Akaishi. *Phys. Lett.* **B535** (2002), 70

[13] T. Suzuki *et al.*, *Phys. Lett.* **B597** (2004), 263

[14] M. Sato *et al.*, arXiv:nucl-ex/0808.2968v1

[15] V. Magas *et al.*, *Phys. Rev.* **C74** (2006), 0205206

[16] This work is part of the PhD Thesis of H. Fujioka, University of Tokyo

[17] S. Piano in HADRON07 Conference (Frascati, October 2007), to be published in *E.P.J.*

[18] FINUDA Collaboration, M. Agnello *et al.*, *Phys. Lett.* **B654** (2007), 80